Research Article | Vol. 27, No. 16 / 5 August 2019 / Optics Express A1188
Optics EXPRESS

Calibration of the LISST-VSF to derive the volume scattering functions in clear waters

LIANBO HU,[1,2] XIAODONG ZHANG,[3,*] YUANHENG XIONG,[1] AND MING-XIA HE[2]

[1] Department of Earth System Science and Policy, University of North Dakota, Grand Forks, ND 58203, USA
[2] Ocean Remote Sensing Institute, Ocean University of China, Qingdao, 266003, China
[3] Division of Marine Science, University of Southern Mississippi, Stennis Space Center, Mississippi 39539, USA
[*] Xiaodong.zhang@usm.edu

Abstract: The recently commercialized LISST-VSF instrument measures the volume scattering function (VSF) from 0.1° to 15° with a traditional laser diffraction unit (LISST) and from 15° to 155° with an eyeball component. Between these two optical components, only the LISST unit is calibrated. The eyeball measurements are scaled using the VSFs at 15° that are measured by both components. As this relative calibration relies on a valid measurement at 15° by the LISST, it might fail in clear oceanic waters, where the forward scattering is relative weak either due to a lack of large particles or an overall low concentration of all particles. In this study, we calibrated the LISST-VSF eyeball component through a series of lab experiments using standard polystyrene beads. Validation with the beads of two different sizes showed a median difference of 11.1% between theoretical and calibrated values. Further evaluations with *in situ* data collected by the LISST-VSF and an ECO-BB3 meter indicated that the new calibration worked well in both turbid and clear waters, while the relative calibration method tended to overestimate VSFs in clear waters.

1. Introduction

The volume scattering function (VSF) and the absorption coefficient are two fundamental inherent optical properties. The VSF ($\beta(\theta)$, m^{-1} sr^{-1}) is defined as the radiant intensity, $I(\theta)$, scattered at a scattering angle θ per incident irradiance (E) and per unit volume of water (Δv) [1].

$$\beta(\theta) = \lim_{\Delta v \to 0} \frac{I(\theta)}{E \Delta v} \tag{1}$$

In the aquatic environment, the VSF is usually partitioned into the contributions by pure water or seawater, dissolved compounds, and suspended particles. The VSF by pure water and associated sea salts can be predicted reasonably well, agreeing with the measurements within 2% [2–4], whereas significant uncertainties exist for the VSFs associated with suspended particles and dissolved compounds. While the absorption coefficients of seawater have been routinely measured in the field, thanks to the commercially available absorption-attenuation meters [5], *in situ* VSF measurements were scarce primarily because of engineering difficulties and hence a lack of commercial instruments. The pioneering work of VSF measurements started more than a half century ago [6–8]. Among them, the VSFs measured by Petzold in 1971 using two separate scattering meters covering an angular range from 0.1° to 170° [6] in three types of water (i.e., open ocean, coastal and harbor waters) were widely adopted by ocean optics and ocean color communities in radiative transfer simulation and ocean color algorithm development (e.g.,[9–11]). In the 80s and 90s, measurements on polarized scattering of oceanic waters [12] and of some specific marine species [13–17] were reported. In the last two decades, the advance in modern optical technology led to the development of several prototype VSF instruments [18–26]. Lee

#366045 https://doi.org/10.1364/OE.27.0A1188
Journal © 2019 Received 24 Apr 2019; revised 3 Jul 2019; accepted 3 Jul 2019; published 19 Jul 2019

Optics EXPRESS

and Lewis [18] developed a Volume Scattering Meter (VSM) with a periscope-shaped prism measuring the VSF from 0.6° to 177.3° with an angular resolution of 0.3°. WETLab developed a Multi-Angle Scattering Optical Tool (MASCOT) measuring the VSF between 10° and 170° at 10° intervals with a sampling frequency up to 20 Hz [21]. Tan et al. [25] presented a novel VSF instrument design using an imaging detector capable of acquiring the VSF from 8° to 172° at 1° interval in a few seconds. More recently, Chami et al. [26] developed a Polarized Volume Scattering Meter (POLVSM) measuring the VSF from 1° to 179° as well as eight additional Mueller scattering matrix elements. These custom-built prototype instruments, despite their improved capabilities in resolving the VSFs in the natural environment, are generally inaccessible to wider research communities for routine observation and investigation.

LISST-VSF developed by Sequoia Scientific Inc. is the first commercial *in situ* instrument capable of measuring the VSF (i.e., P_{11}) in the aquatic environment over a wide angular range from 0.1° to 155° as well as the P_{12} and P_{22} elements of the Mueller scattering matrix from 15° to 155° [27,28]. A LISST-VSF consists of two optical components, a laser diffraction unit (LISST) and an eyeball component. The LISST unit measures the VSF at angles $< 15°$ using the ring detectors identical to LISST-100X/200X in design and is calibrated [29,30]. The eyeball component measures the VSF at angles $\geq 15°$ with two photomultiplier tubes (PMT) and is not calibrated. The light source of LISST-VSF is a single wavelength TE-cooled diode laser. During data acquisition, the laser beam is rapidly chopped on and off such that both scattering signal and background noise (due to ambient light and dark current) are recorded. The difference of these two measurements is used for further analysis. Also, the laser is dimmed for eyeball measurements at scattering angles between 15° and 50° to reduce the intensity of forward-scattered light at these angles; it remains in full intensity for the rest eyeball measurements as well as for the ring data recording. A full angular scattering measurement takes about four seconds.

The default data processing implemented in the LISST-VSF software adopts an *ad hoc* approach to calibrate the eyeball measurements. The idea is to use the VSFs measured by the LISST ring detectors, which are calibrated, to scale the measurements by the eyeball component. Specifically, after converting signal recorded by the LISST ring detectors to the VSFs, their values at 12.3° and 14.4° (by the two outermost rings) are linearly extrapolated to 15°. Then, a scaling factor is computed between this extrapolated VSF at 15° and the eyeball signal at the same angle. Finally, the scaling factor is applied to the eyeball signal at other scattering angles to calculate the VSFs. There are two issues in this relative calibration method. First, there is no theoretical basis for linear dependency of angular scattering at these angles, even though an inverse power law has been used to approximate VSFs at small angles [31,32] and observed in the field measurement of natural waters [6]. Second, this calibration method relies on the performance of the two outermost ring detectors. If one of them suffers a malfunction or a greater uncertainty, the entire measurement of the eyeball component is affected. For example, we found the measurements collected in clear oceanic waters by the two outermost rings frequently exhibit a greater variability than in more turbid waters, making the extrapolation to estimate the VSF at 15° unreliable and directly affecting the subsequent relative calibration of the eyeball measurements.

The default data processing also involves the use of a blank, which is subtracted from the raw signal before further processing. While the use of a blank does not affect the relative calibration of the eyeball measurements as long as the blank is consistently used for both LISST-VSF ring detectors and the eyeball unit, it does introduce additional issues depending on how the blank is prepared. For example, if a blank that is prepared in the laboratory to represent the scattering by pure water is used in the field, the remaining scattering would represent a strange combination of the scattering by particles plus the scattering due to the presence of sea salts. To avoid this, a blank is often prepared during a field experiment by filtering the seawater with a filter of pore size of 0.2 µm. This approach avoids the "strange" scattering but incurs two additional issues. First, it would preclude any possibility to study particles of sizes < 0.2 µm, which could play a significant

Optics EXPRESS

role in backscattering [33–36]. Second, depending on the source of the blank, sometimes this blank subtraction could lead to unphysical, negative values, which we have experienced ourselves.

The objective of this study is two-fold. First, we need to develop an alternative calibration method for the LISST-VSF eyeball component independent of LISST ring detectors such that the LISST-VSF instrument can be used in both clear and turbid waters. Second, we want to test the performance the LISST-VSF in the field without using the blank. The structure of this manuscript is organized as follows. First, the data processing for the LISST-VSF eyeball component and the relative calibration method provided by the manufacturer were explained, followed by the introduction of the calibration method developed in this study and the calibration experiments. The calibration coefficient was derived from the standard polystyrene bead with a nominal diameter of 0.2 μm and validated with the beads of different sizes. Finally, the calibration developed in this study was evaluated using *in situ* data collected by the LISST-VSF in three cruises by comparing with the relative calibration method and the independent measurements.

2. Data and methodology

2.1. Overview of data processing of the LISST-VSF eyeball measurements

The LISST-VSF eyeball component measures the intensity and polarization state of the scattered light. The laser of our LISST-VSF operates at a center wavelength of 517 nm. The laser polarization is alternated between vertical and horizontal states by insertion or removal of a half-wave plate. The vertical and horizontal components of scattered light are separated by a polarizing beam splitter and recorded by two PMT detectors [27]. In this setup, four different combinations of linear polarization between the incident and the scattered light are measured at scattering angles between 15° and 155°. The first batch of processing for the raw data recorded by two PMTs includes removal of the background noises, correction of the changes in the viewing geometry, correction of the dimming of the laser power, and correction for light attenuation through the medium and the optical components. This process can be summarized as:

$$I_{ij}(\theta, V) = [I_{ij}^{\text{on}}(\theta, V) - I_{ij}^{\text{off}}(\theta, V)]e^{cL(\theta)}T_{\text{v}}\sin(\theta)f(\theta_{15^{\text{o}}-50^{\text{o}}}), \quad \begin{matrix} i = \text{h,v} \\ j = \text{h,v} \end{matrix} \tag{2}$$

where I represents the scattered light in digital count, the superscripts on and off indicate signal recorded by PMT when laser is chopped on and off, respectively, the subscripts v and h indicate vertical and horizontal polarization with the first indicating the polarization state of the laser beam and the second the polarization state of the scattered light, θ is scattering angle, V is the PMT supply voltage (i.e., PMT gain), c is the attenuation coefficient of the sample directly measured by a photodiode centered at zero scattering angle, $L(\theta)$ is the path length along the laser beam through the scattering volume then to the PMT detectors, T_{v} is the transmittance of the half-wave plate, which only applies to the measurements with the vertically polarized incident light (i.e., I_{vh} and I_{vv}), $\sin(\theta)$ describes the relative change of the viewing volume with θ, and $f(\theta_{15^{\circ}-50^{\circ}})$ is the laser dimming factor that only applies to the measurements between 15° and 50°.

I_{ij} calculated from Eq. (2) are related to the Mueller scattering matrix elements of P_{11} (i.e., VSF), P_{12}, and P_{22} [37,38] as:

$$\begin{aligned}
\kappa(\theta, V)I_{\text{hh}}(\theta, V)/I_0 &= P_{11}(\theta) + P_{12}(\theta) + \cos(2\theta)[P_{12}(\theta) + P_{22}(\theta)], \\
\kappa(\theta, V)I_{\text{hv}}(\theta, V)/I_0 &= \alpha\{P_{11}(\theta) + P_{12}(\theta) - \cos(2\theta)[P_{12}(\theta) + P_{22}(\theta)]\}, \\
\kappa(\theta, V)I_{\text{vh}}(\theta, V)/I_0 &= P_{11}(\theta) - P_{12}(\theta) + \cos(2\theta)[P_{12}(\theta) - P_{22}(\theta)], \\
\kappa(\theta, V)I_{\text{vv}}(\theta, V)/I_0 &= \alpha\{P_{11}(\theta) - P_{12}(\theta) - \cos(2\theta)[P_{12}(\theta) - P_{22}(\theta)]\},
\end{aligned} \tag{3}$$

Optics EXPRESS

where I_0 is the incident light intensity in digital counts, α is the sensitivity ratio of the two PMTs, and $\kappa(\theta, V)$ is the lump-sum calibration coefficient to be determined, accounting for the quantum efficiency of the optical components (the PMTs and the photodiode) and the laser-receiver geometry. Theoretically, $\kappa(\theta,V)$ should be independent of scattering angle after correcting for the path attenuation and the change in the scattering volume with the scattering angle (Eq. (2)). Solving Eq. (3), we have,

$$P_{11}(\theta) = \beta(\theta) = \kappa(\theta, V)P_{11}^{\text{uncal}}(\theta, V), \tag{4}$$

and

$$P_{11}^{\text{uncal}}(\theta, V) = [I_{\text{hh}}(\theta, V) + I_{\text{hv}}(\theta, V)/\alpha + I_{\text{vh}}(\theta, V) + I_{\text{vv}}(\theta, V)/\alpha]/4I_0, \tag{5}$$

where $P_{11}^{\text{uncal}}(\theta, V)$ represents uncalibrated P_{11} at a given PMT supply voltage of V. Similarly, we have,

$$P_{12}(\theta) = \kappa(\theta, V)P_{12}^{\text{uncal}}(\theta, V), \tag{6}$$

$$P_{12}^{\text{uncal}}(\theta, V) = [I_{\text{hh}}(\theta, V) - I_{\text{vh}}(\theta, V) + I_{\text{hv}}(\theta, V)/\alpha - I_{\text{vv}}(\theta, V)/\alpha]/4I_0, \tag{7}$$

where $P_{12}^{\text{uncal}}(\theta, V)$ represents uncalibrated P_{12} at a given PMT supply voltage of V. As expected with the LISST-VSF instrument, which uses the same detectors to measure the Mueller scattering matrix elements, the calibration coefficient $\kappa(\theta, V)$ for P_{12} (and P_{22}, not shown) is the same as for P_{11}.

2.2. The default, relative calibration for eyeball measurements

The relative calibration method for P_{11} provided by the manufacturer was briefly described above. Mathematically, this calibration method can be expressed as follows:

$$\beta^{\text{LISST}}(15^\circ) = 1.29\beta^{\text{LISST}}(14.4^\circ) - 0.29\beta^{\text{LISST}}(12.3^\circ), \tag{8}$$

$$SF(V) = \beta^{\text{LISST}}(15^\circ)/P_{11}^{\text{uncal}}(15^\circ, V), \tag{9}$$

$$\beta^{\text{eyeball}}(\theta) = SF(V)P_{11}^{\text{uncal}}(\theta, V), \tag{10}$$

where β^{LISST} represents the VSF measured by the LISST-VSF ring detectors, which are calibrated, β^{eyeball} represents the VSF measured by the LISST-VSF eyeball component, and $SF(V)$ is the scaling factor corresponding to the PMT supply voltage V.

2.3. Absolute calibration for eyeball measurements

In order to measure VSFs in different waters, a LISST-VSF uses 10 PMT supply voltage steps, from a minimum of 400 mV to a maximum of 820 mV, to provide 10 different gain values from approximately 700 to 350,000. The gain of a PMT is the ratio of the anode current to the photocathode current and varies as

$$G_2/G_1 = (V_2/V_1)^\gamma, \tag{11}$$

where G_2 and G_1 are the PMT gains at supply voltages V_2 and V_1, γ is a coefficient determined by the dynode material and the geometry. For our specific LISST-VSF (SN = 1662), $\gamma = 8.6$ according to the specification provided by the PMT manufacturer. The actual PMT supply voltage is automatically selected during operation such that the amplified signal is within the optimal range of the detectors. While it is possible to develop a set of calibration coefficients $\kappa(\theta,V)$ for each of 10 PMT gain settings, we chose to develop one set of calibration coefficients

Optics EXPRESS

for one reference PMT voltage by converting $P_{11}^{\text{uncal}}(\theta, V)$ at different voltages to one reference voltage,(V_0) i.e.,

$$P_{11}^{\text{uncal}}(\theta, V_0) = P_{11}^{\text{uncal}}(\theta, V)(V_0/V)^{\gamma}. \tag{12}$$

In this study, the PMT supply voltage at 645 mV was chosen as the reference voltage (i.e., $V_0 = 645$ mV) because this PMT supply voltage was automatically selected in > 95% of the measurements collected in clear oceanic waters (see section 4.1).

Combining Eq. (4) and Eq. (12), we have

$$\beta^{\text{eyeball}}(\theta) = \kappa(\theta, 645\text{mV})P_{11}^{\text{uncal}}(\theta, 645\text{mV}). \tag{13}$$

Absolute calibration is to apply $\kappa(\theta$,645 mV) using Eq. (13) to calculate the VSFs. Also, we used Eq. (13) to determine $\kappa(\theta$,645 mV) in the lab experiments using standard beads, for which $\beta^{\text{eyeball}}(\theta)$ can be computed.

2.4. Use of a blank

In a controlled experiment, such as the bead experiments we described below, subtraction of a blank is necessary because the blank was clearly defined, which represents the scattering of water before beads were added. If a blank is used, the data processing for the blank is the same as Eq. (2), which in this case produces $I_{ij}^{\text{b}}(\theta, V)$. The subtraction of the blank is performed as:

$$I_{ij}^{\text{nb}}(\theta, V) = I_{ij}(\theta, V) - I_{ij}^{\text{b}}(\theta, V). \tag{14}$$

The subsequent data analysis of I_{ij}^{nb} and its calibration is the same from Eqs. (3) – (13), except that the resulting $\beta_{\text{nb}}(\theta)$ now represents the corresponding non-blank VSF. If the relative calibration is used, the same blank should also be subtracted from the ring measurements before calculating the scaling factor. In the following, a quantity with a subscript "nb" indicates the quantity is derived with blank-subtraction.

2.5. Calculation of particulate VSF (β_p)

Instead of using a blank, the particulate VSF (β_{p}) in the field experiments can also be easily calculated by subtracting the VSF of pure water or pure seawater (β_{sw}) predicted by the theoretical model [2–4], i.e.,

$$\beta_{\text{p}}(\theta) = \beta(\theta) - \beta_{\text{sw}}(\theta). \tag{15}$$

Strictly speaking, only $\beta_{\text{p}}(\theta)$ derived in this way represents true particulate scattering, i.e., scattering due to non-water particles and is consistent with the particulate scattering derived from many other commercial scattering instruments, such as the Sea-Bird/WETLab backscatter sensors [39–41]. If both β_{p} and β_{nb} are measured, β_{p} should be greater than β_{nb}, at least theoretically, because a blank always contains particles, no matter how carefully it is prepared.

2.6. Calibration experiments

The polystyrene beads with known refractive index and size distribution are commonly used to calibrate VSF instruments [18,25,26,41–43]. As these artificial monodispersed particles are more or less spherical with known size and refractive index, their scattering can be computed using Mie theory [44]. The polystyrene beads (Duke STANDARDS$^{\text{TM}}$) with various sizes were ordered from Thermo Fisher Scientific Inc. The specifications of polystyrene beads used in this study are listed in Table 1. A population of beads of nominal diameter (μ_{ND}) is assumed to be normally distributed with an actual mean diameter of μ_{D} and a standard deviation of σ_{D}. The estimate of the actual mean diameter is traceable to National Institute of Standard and Technology (NIST) and has an uncertainty of δ_{D} at 95% confidence level. According to the manufacturer

Optics EXPRESS

(Thermo Fisher), the real part of the refractive index of the polystyrene beads (n_r) and their concentration in the original suspension (N_0) can be estimated as,

$$n_r(\lambda) = 1.5663 + 0.00785/\lambda^2 + 0.000334/\lambda^4, \tag{16}$$

and

$$N_0 = 6\rho_w/\pi/(\mu_D^3 + \sigma_D^3)/(\rho_w - \rho_p + \rho_p/C_p), \tag{17}$$

Table 1. The specification of polystyrene beads used in this study. Beads of a nominal diameter μ_{ND} are assumed to be normally distributed with an actual mean diameter of μ_D and a standard deviation of σ_D. δ_D represents the uncertainty in determining μ_D at 95% confidence level. The complex refractive index (n) and the original concentration (N_0) calculated at 517 nm for different bead suspensions are also listed.

μ_{ND} (μm)	μ_D (μm)	δ_D (μm)	σ_D (μm)	n	N_0 (m^{-3})
0.2	0.203	0.005	0.0053	1.6003+ (0.00035 ± 0.00015) i	2.18×10^{18}
0.5	0.508	0.008	0.0085	1.6003+ (0.00035 ± 0.00015) i	1.39×10^{17}
11.0	11.1	0.5	0.6	1.6003+ (0.00035 ± 0.00015) i	1.33×10^{13}

respectively, where λ is the wavelength in vacuum in unit of μm, ρ represents density, whose subscripts w and p represent water and particles (beads), respectively, and C_p is the mass ratio of the beads. The imaginary part of the refractive index of beads is small in the visible wavelengths [45] and its effects on scattering were usually neglected [18,25,26]. This assumption holds true for beads of smaller sizes (e.g.,< 2 μm) but fails for beads of larger sizes [42]. In this study, we used a value of 0.00035 ± 0.00015 for the imaginary part of the refractive index following Ma et al. [45].

To calculate the bulk optical properties of a bead suspension using Mie theory, the solution needs to be sufficiently dilute to meet single-scattering condition. In the radiative transfer theory, one attenuation length has been long regarded as a rule of thumb for single scattering approximations [46,47]. The path length of laser beam of the LISST-VSF varies with the viewing angle, ranging from 10 to 20 cm; therefore, the criterion is that the attenuation coefficient of the sample should be $< 5\ m^{-1}$. The volume scattering function of an assemblage of beads (β^{Mie}) with a known size distribution (φ) is calculated as:

$$\beta^{Mie}(\theta) = N \int_{\mu_D-3\sigma_D}^{\mu_D+3\sigma_D} S^{Mie}(\theta, D)\varphi(D)dD, \tag{18}$$

where S^{Mie} represents the scattering cross section calculated from Mie theory, N is the concentration of polystyrene beads in the sample (m^{-3}), D is the diameter of the beads, and φ is normalized Gaussian function. β^{Mie} computed for the three bead populations listed in Table 1 and normalized by the total scattering integrated from 15° to 155° are shown in Fig. 1. We applied a Monte Carlo method to evaluate the impact of the uncertainties in the mean diameter and the imaginary part of the refractive index of the beads on the calculation of β^{Mie} [42]. Specifically, a normally distributed population of beads were generated with its mean diameter varying within $\mu_D \pm \delta_D$ and the imaginary refractive index varying within 0.00035 ± 0.00015. We perturbed the population 2000 times and for each of these perturbations, β^{Mie} is calculated using Eq. (18). For the three polystyrene beads populations with a nominal diameter of 0.2 μm, 0.5 μm, and 11.0 μm, the impacts of uncertainties (measured as the coefficient of variation) in the mean diameter on β^{Mie} (Fig. 1(a)) are 4.3%, 4.9%, and 3.5% , respectively; the impacts of uncertainties in the imaginary refractive index on β^{Mie} (Fig. 1(b)) are 0.02%, 0.1%, and 2.0%, respectively.

In principle, the calibration of the LISST-VSF instrument, or any other scattering sensors, should not depend on the exact size of beads used in calibration. In this study, we used beads of

Optics EXPRESS

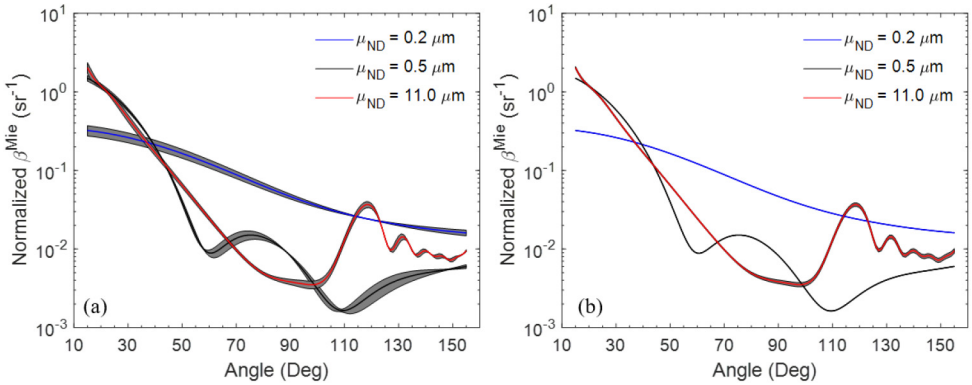

Fig. 1. Variations of the VSF (β^{Mie}) calculated for the three polystyrene beads listed in Table 1 with perturbations in their mean diameter (a) and their imaginary part of the refractive index (b). To ease comparison, the β^{Mie} values are normalized by the total scattering intergraded from 15° to 155°.

nominal diameter of 0.2 µm for calibration and two larger-sized beads for validation because, as shown in Fig. 1, smaller beads produce a relatively featureless pattern of angular scattering whereas beads of larger sizes exhibit ripples in the angular scattering that are very sensitive to the precise size and refractive index of the beads, making calibration with larger beadsat those angles difficult. Also, larger beads show a strong forward scattering and hence a relative weak backscattering. To effectively calibrate the LISST-VSF with larger beads at backward scattering angles often requires a concentration that is too high such that the multiple scattering can no longer be ignored.

The calibration experiment was conducted with the LISST-VSF in benchtop mode. A plastic sheet equipped with a magnetic stir bar was wrapped around the sample chamber and fixed with clamps over the gasket strips. The optical windows, inner endcaps and chamber were thoroughly rinsed using Ultrapure water (MilliporeSigma Direct-Q 3UV). Two liter Ultrapure water were recirculated through a polycarbonate cartridge filter of pore size 0.2 µm for 30 minutes to further remove residual particle contaminations. We will refer to Ultrapure water prepared this way as pure water. A master solution of 0.2 µm beads was prepared by adding 100 µL of the original bead suspension into 30 mL of pure water. This master bead solution has a concentration of 6.57×10^{15} m^{-3} and a scattering coefficient of 33 m^{-1}. The original bead suspension was agitated in advance by hand as well as on a vortex mixer to homogenize the suspension and break down possible aggregation of particles. 1.6 L of pure water was added to the LISST-VSF sample chamber and its VSF was measured to serve as the blank. Subsequently, a 2 mL of bead master solution was added into the chamber sequentially. After each addition, the magnetic bar was turned on for two minutes to homogenize the beads in the chamber before taking 30 measurements of the VSFs. We repeated this procedure 10 times, producing a series of solutions with concentrations varying from 8.1×10^{12} to 8.0×10^{13} m^{-3}, the scattering coefficients from 0.05 to 0.5 m^{-1}, and the backscattering coefficients from 0.006 to 0.06 m^{-1}. This range of the backscattering coefficients covers the typical variability of oceanic waters [48] and the range of total scattering coefficients indicate the samples are well within the single-scattering regime. The experiments using the other two polystyrene beads (μ_{ND} = 0.5 µm and μ_{ND} = 11.0 µm) were conducted similarly.

2.7. *In situ data collection*

The LISST-VSF was used in three field experiments; two with the Line P Program conducted in June 2017 (LP-2017) and February 2018 (LP-2018), respectively, and the third with the

Optics EXPRESS

EXPORTS (EXport Processes in the Ocean from Remote Sensing) experiment conducted in August of 2018 (EX-2018). The LP-2017 and LP-2018 experiments surveyed three stations (i.e., SG41, HARO59 and JF2) in the Salish sea and other 26 stations (red dots in Fig. 2) along a transect stretching from the southern tip of Vancouver Island in British Columbia (P1, 125.5°W, 48.5°N) to the Ocean Station Papa (OSP; P26, 145°W, 50°N) [49]. The Line P covers a variety of water types ranging from sediment-dominated turbid coastal waters to clear North Pacific Ocean waters [50]. The EXPORTS experiment was a large-scale NASA-led field campaign aiming to quantify export and fate of upper ocean net primary production using both satellite and *in situ* observations [51]. The EX-2018 stations were bounded within 144°-145.8°W and 49.6°-51.2°N (black rectangle in Fig. 2). During these three experiments, the LISST-VSF was operated in benchtop mode measuring discrete water samples collected by CTD casts at various depths. In EX-2018, the scattering of seawater samples after 0.2 µm filtration were also measured to evaluate the contribution of very small particles (< 0.2 µm) to total particulate backscattering.

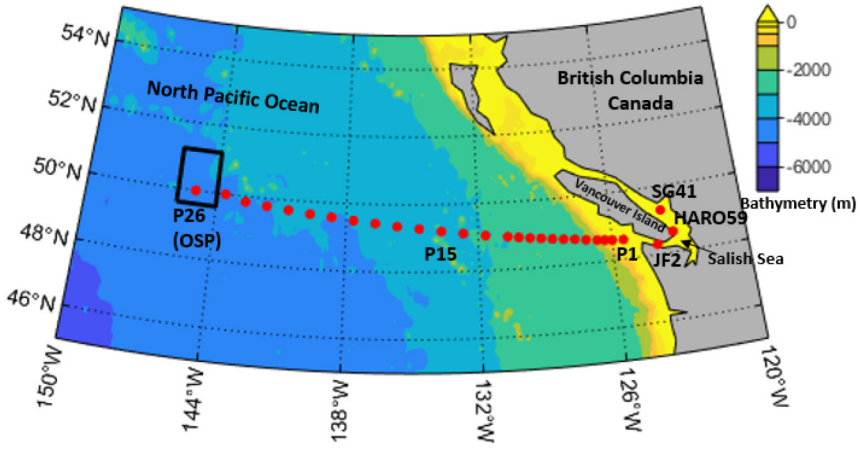

Fig. 2. Stations of Line P Program (red dots) and boundary of the EXPORTS 2018 experiment (black rectangle around P26). The background is bathymetry of the study area.

3. Results

In all the laboratory and field experiments, 30 measurements were taken for each sample. For the lab experiments using beads, for which a blank could be clearly defined as the water before adding beads, the data were processed by subtracting the blank. For the field experiments, for which a blank is difficult to define, the bulk data were processed directly. We used median values of these repeated measurements for further analysis.

3.1. Calibration with 0.2 µm beads

Throughout the measurements, only three PMT gains of 595, 645, and 700 mV were selected automatically. Figure 3(a) shows, as an example, the correlation obtained from the 10 samples between gain-converted $P_{11}^{\text{uncal}}(\theta, 645\text{mV})$ and simulated $\beta^{\text{Mie}}(\theta)$ at a scattering angle of 60°. Calculated $P_{11}^{\text{uncal}}(\theta, 645\text{mV})$ exhibited a nearly perfect linear relationship with $\beta^{\text{Mie}}(\theta)$ with a Pearson correlation coefficient $r > 0.99$. The standard deviation of 30 repeated measurements at each concentration (represented by horizontal bars in Fig. 3(a)) varies from 0.4% at higher concentrations to 6.6% at lower concentrations with an average of 1.5%, suggesting the beads were well mixed during the experiments. The standard deviation of $\beta^{\text{Mie}}(\theta)$ due to uncertainty in the mean diameter (represented by vertical bars in Fig. 3(a)) is 4.3% for all concentrations.

Optics EXPRESS

At each scattering angle, calibration coefficient $\kappa(\theta,645\,\mathrm{mV})$ was derived as the slope between $P_{11}^{\mathrm{uncal}}(\theta,645\mathrm{mV})$ and $\beta^{\mathrm{Mie}}(\theta)$ by applying a robust linear regression model [52] (Fig. 3(b)).

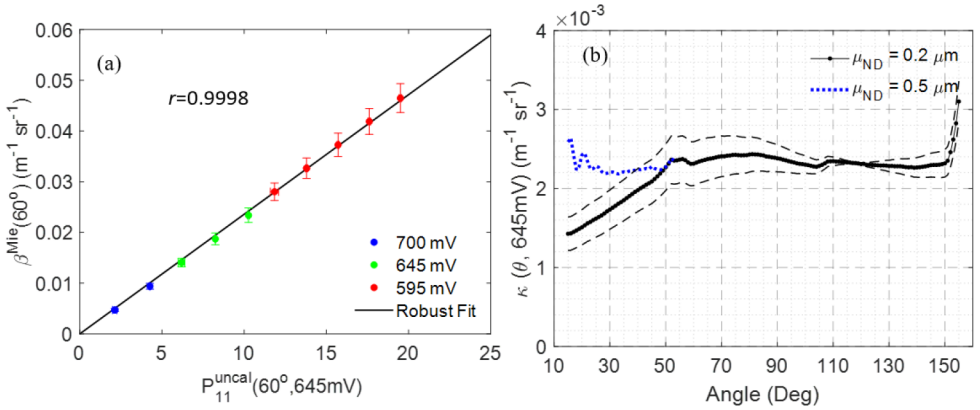

Fig. 3. (a) Scatter plot between $P_{11}^{\mathrm{uncal}}(60°, 645\mathrm{mV})$ measured by the LISST-VSF eyeball component and $\beta^{\mathrm{Mie}}(60°)$ calculated for polystyrene beads ($\mu_{ND} = 0.2$ μm) at 10 concentrations. Horizontal and vertical error bars represent standard deviations estimated, respectively, from the 30 measurements of $P_{11}^{\mathrm{uncal}}(60°, 645\mathrm{mV})$ at each concentration and from $\beta^{\mathrm{Mie}}(60°)$ calculated by accounting for uncertainties in the mean diameter of the beads. The uncertainties associated with the imaginary part of the refractive index of the 0.2 μm beads are negligible and hence ignored. Blue, green, and red colors correspond to three different PMT supply voltages that were automatically selected during the measurements. (b) Calibration coefficients $\kappa(\theta,645\,\mathrm{mV})$ estimated as the linear slope between $P_{11}^{\mathrm{uncal}}(\theta, 645\mathrm{mV})$ and $\beta^{\mathrm{Mie}}(\theta)$ at each scattering angle. The solid line represents the median values and two dash lines indicate the 95% confidence interval. The dotted blue line represents $\kappa(\theta,645\,\mathrm{mV})$ between 15° and 50° derived from 0.5 μm beads .

The estimated $\kappa(\theta,645\,\mathrm{mV})$ changed slightly from 50° to 150°, varying from 2.27×10^{-3} to 2.42×10^{-3} m^{-1} sr^{-1} with an average of 2.30×10^{-3} m^{-1} sr^{-1}. Interestingly, this average value obtained over angles from 50° to 150° is almost the same as the average value obtained from 110° to 130°, over which the derived $\kappa(\theta,645\,\mathrm{mV})$ showed the least uncertainty (see dashed lines in Fig. 3(b)). A conspicuous decrease of $\kappa(\theta,645\,\mathrm{mV})$) was observed at angles < 50°, reaching a minimum of 1.43×10^{-3} m^{-1} sr^{-1} at 15°. The similar pattern of $\kappa(\theta,645\,\mathrm{mV})$ at angles < 50° also showed up when using beads with nominal diameter of 0.15 μm but was not observed when using beads of larger sizes. For example, the blue dotted line in Fig. 3(b) was obtained with beads of nominal diameter of 0.5 μm. Initially we thought this was probably due to the dimming of the laser at angles from 15° to 50°. We turned off the dimming, but obtained the same results (not shown). Discussion with the manufacturer was also inconclusive. The increase of $\kappa(\theta,645\,\mathrm{mV})$ for angles >150° was likely caused by the contamination of stray light reflected by the receiving window (personal communication with David Danna with Sequoia Scientific Inc.). Data measured by the LISST-VSF at those angles are discarded. As the LISST-VSF eyeball component uses a single detector, $\kappa(\theta,645\,\mathrm{mV})$ should be invariant with the scattering angle if the changes in the path attenuation and the scattering volume are corrected as in Eq. (2). This is more or less demonstrated for scattering angles from 50 to 150°. Even though our calibration using 0.2 μm showed $\kappa(\theta,645\,\mathrm{mV})$ decreasing from 50° to 15°, this pattern was not observed when testing with beads of larger sizes. Therefore, we decided to use a fixed value of 2.30×10^{-3} m^{-1} sr^{-1} for $\kappa(\theta,645\,\mathrm{mV})$ for θ from 15° to 150°.

Optics EXPRESS

3.2. Validation with 0.5 μm and 11.0 μm beads

Measurements for polystyrene beads of nominal diameters of 0.5 μm and 11.0 μm, each at 10 different concentrations, were used for validation. The blank representing pure water before beads were added was subtracted. $\beta_{nb,rel}(\theta \geq 15°)$ values were calculated using the relative calibration and $\beta_{nb,abs}(\theta \geq 15°)$ values were calculated using the absolute calibration coefficient $\kappa(645\,mV) = 2.30\times10^{-3}$ m^{-1} sr^{-1} determined in section 3.1.

An example of validation is shown in Fig. 4(a) for the 0.5 μm bead sample with a concentration of $b_{bp} = 5.8\times10^{-4}$ m^{-1}, which is comparable in value to the backscattering observed in the central gyre in the Southeast Pacific Ocean [48]. $\beta_{nb,abs}(\theta \geq 15°)$ (blue dots) agreed well with the Mie-predicted values, whereas $\beta_{nb,rel}$ $(\theta \geq 15°)$ (black dots) were overestimated by on average a factor of 2.5. Examination of β_{nb} $(\theta < 15°)$ (green dots) obtained from the LISST-VSF ring detectors indicates clearly that this overestimation resulted from the abnormally elevated β_{nb} (12.3°) and β_{nb} (14.4°), leading to doubtful extrapolation to $\beta_{nb}(15°)$ and thereby the scaled eyeball measurement. Actually, all $\beta_{nb}(\theta < 15°)$ measured by the LISST-VSF ring detectors are doubtful in this case because the forward scattering generated by 0.5 μm beads were too weak to be detected by the LISST-VSF ring detectors. Another example of validation is shown in Fig. 4(b) for the 11.0 μm beads at a relatively higher concentration with $b_{bp} = 0.012\,m^{-1}$. Similarly, $\beta_{nb,abs}$ $(\theta \geq 15°)$ (blue dots) agreed well with the predicted values. Unlike the validation shown in Fig. 4(a), both $\beta_{nb}(\theta < 15°)$ measured by the LISST-VSF ring detectors and $\beta_{nb,rel}$ $(\theta \geq 15°)$ agreed well with the Mie prediction, which also indicates that the default, relative calibration provided by Sequoia for the LISST-VSF ring detectors works for the experiment using 11 μm beads. The contrast of these two examples reveals that the relative calibration method only works in waters with sufficient forward scattering but might fail in waters with insufficient forward scattering, which is often the case in clear oceanic waters with an overall low particle concentration and/or a lack of large particles. Evaluated for all the 0.5 μm-bead samples at various concentrations with b_{bp} varying from 5.8×10^{-4} to 5.8×10^{-3} m^{-1}, the absolute calibration has an uncertainty (measured by the relative percentage difference (RPD)) < 12% at all scattering angles with an average of 8.5% (blue curve in Fig. 4(c)). Evaluated for all the 11.0 μm-bead samples with b_{bp} varying from 0.0012 to 0.012 m^{-1}, RPD is generally < 20% except at angles from 80° to 110° and has an average value of 13.8% (red curve in Fig. 4(c)). Overall, applying the absolute calibration coefficient determined in this study to the measurements by the LISST-VSF eyeball component could retrieve the VSFs with a correlation coefficient $r > 0.99$ and an overall uncertainty of 11.1% (Fig. 4(d)).

In this study, the absolute calibration coefficient $\kappa(645\,mV)$ was determined from the measurements of the Mueller scattering matrix element P_{11}. As we expect the same coefficient also applies to P_{12}, we further evaluated the calibration applied to P_{12} in Fig. 4(e) and (f) for 0.5 μm and 11.0 μm beads, respectively. For both sizes, P_{12} calibrated using $\kappa(645\,mV)$ (blue dots) agreed very well with Mie-predicted values (red line) at scattering angles >50°. At angles <50°, some discrepancies were observed for both comparison, which, we believe, were caused by the laser dimming for $\theta < 50°$. In order to reduce the high scattering intensity of VSF (i.e., P_{11}) at forward angles, the laser beam was dimmed 12-fold at angles $\theta < 50°$. Unlike P_{11}, P_{12} does not show high intensity at these angles however; therefore, the laser dimming ends up reducing the signal-to-noise ratio for P_{12} at these angles. Indeed, a better comparison was observed for P_{12} at angles <50° when laser dimming was turned off (data not shown).

3.3. Application to in situ measurements

3.3.1. Comparison with the relative calibration method

The VSFs were measured using the LISST-VSF in three field experiments (Table 2). We processed the bulk LISST-VSF measurements using Eq. (15) to calculate $\beta_{p,abs}(\theta)$ with the

Optics EXPRESS

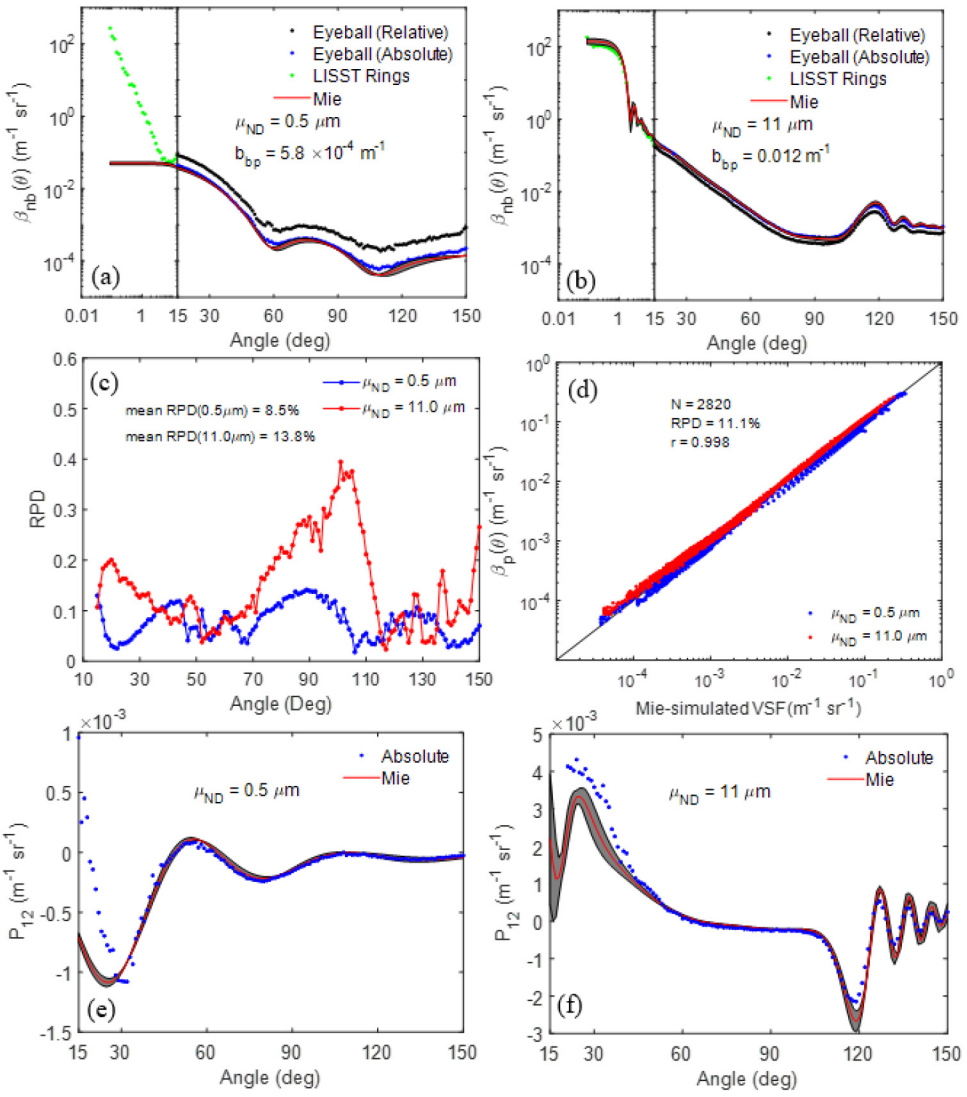

Fig. 4. (a) Comparison of non-blank VSFs (β_{nb}) at 517 nm measured by the LISST-VSF with Mie-simulated values for the 0.5 µm bead sample with $b_{bp} = 5.8\times10^{-4}$ m^{-1}. Measured β_{nb} include $\beta_{nb,abs}(\theta\geq15°)$ (blue dots) obtained with the LISST-VSF eyeball component using the absolute calibration developed in this study, $\beta_{nb,rel}(\theta\geq15°)$ (black dots) obtained with the eyeball component using the relative calibration, and $\beta_{nb}(\theta<15°)$ obtained with the LISST-VSF ring detectors (green dots). The shaded area represents the perturbations of simulated VSF due to uncertainties associated with mean diameter and imaginary part of the refractive index of beads. The particulate backscattering coefficient (b_{bp}) is calculated from Mie. (b) Same as (a) but for the 11 µm bead sample with $b_{bp} = 0.012$ m^{-1}. (c) Angular evaluation of the absolute calibration in terms of relative percentage difference (RPD) between measured $\beta_{nb,abs}$ and Mie-simulated values. (d) Scatter plot of $\beta_{nb,abs}$ and Mie-simulated values at all scattering angles from 15° to 150° for both 0.5 µm and 11 µm beads, each at 10 concentrations. The overall RPD is 11.1% and the correlation coefficient (r) is 0.998. (e) Comparison of P_{12} measured by the LISST-VSF using the absolute calibration (blue dots) with Mie-simulated values (red line) for the 0.5 µm bead sample. (f) Same as (e) but for the 11 µm bead sample.

Optics EXPRESS

absolute calibration and $\beta_{p,rel}(\theta)$ the relative calibration. Their respective values at 15° are compared in Fig. 5. Overall, $\beta_p(15°)$ calculated with the two calibration methods agreed well for the LP-2017 and LP-2018 experiments with an average difference of 16.6% when $\beta_{p,abs}(15°)$ > 0.1 m^{-1} sr^{-1}, slightly larger than the inherent uncertainty of 11.1% as determined from the validation (Fig. 4(d)). In relatively clear waters where $\beta_{p,abs}(15°) < 0.1$ m^{-1} sr^{-1}, the values of $\beta_{p,rel}(15°)$ were significantly larger than the values of $\beta_{p,abs}(15°)$, with an average difference of 83.2%. This significant discrepancy in $\beta_p(15°)$ between the two calibration methods was also observed in the EX-2018 experiment (black dots in Fig. 5) where all samples were collected in clear waters around OSP station (Fig. 2) and some of them at depths > 300 m. Moreover, $\beta_{p,rel}(15°)$ obtained for the EX-2018 experiment also showed a greater variability than $\beta_{p,abs}(15°)$. For example, the coefficient of variation (CV) of $\beta_{p,abs}(15°)$ is 9.1%, which is more or less expected given the geographic constraint of the EX-2018 stations. In contrast, CV of $\beta_{p,rel}(15°)$ is 141.5%, because the measurements of the two outermost rings that were used to determine relative calibration (Eq. (8)) were very noisy (results not shown).

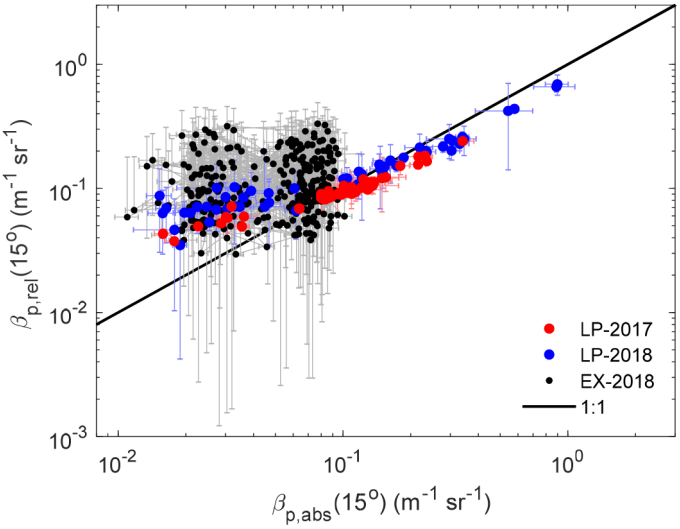

Fig. 5. Comparison of particulate VSF at 15° calculated using the absolute calibration ($\beta_{p,abs}(15°)$) and the relative calibration ($\beta_{p,rel}(15°)$) for the three experiments of LP-2017 (red), LP-2018 (blue), and EX-2018 (black). The error bars represent standard deviations of β_p (15°) estimated from 30 repeated measurements by the LISST-VSF for each sample.

Table 2. The duration of, the number of stations of, and number of seawater samples collected in, each of the three field experiments. The range (median) values of particulate backscattering coefficient (b_{bp}) were calculated for each experiment using the LISST-VSF data with the absolute calibration method and Eq. (19).

Cruise	Date	# of stations	# of samples	b_{bp} (m^{-1})
LP-2017	Jun.4- Jun.20, 2017	28	53	0.0004-0.0080 (0.0015)
LP-2018	Feb.18- Mar.8, 2018	29	52	0.0005-0.0317 (0.0020)
EX-2018	Aug.14 – Sep.10,2018	48	298	0.0004-0.0018 (0.0009)

3.3.2. Comparison with ECO-BB3 measurements

To reconcile the difference seen in Fig. 5, we further compared with the VSF data measured by an ECO-BB3 meter during EX-2018. The ECO-BB3 data were obtained from the NASA's

Optics EXPRESS

SeaWiFS Bio-optical Archive and Storage System (SeaBASS) [53,54]. The ECO-BB3 meter operated in a flow-through mode [55] measuring $\beta_p(124°)$ of seawater collected at approximately 5 m at three wavelengths (470, 532 and 660 nm). For comparison, only ECO-BB3 measurements within 144°-145.8°W and 49.6°-51.2°N (black rectangle in Fig. 2) and near-surface LISST-VSF measurements were used. There were a total of 41 LISST-VSF measurements and 26045 ECO-BB3 measurements that met the above criteria. Furthermore, $\beta_p(124°)$ values from the ECO-BB3 at 470 nm and 532 nm were linearly interpolated to estimate $\beta_p(124°)$ at 517 nm, and $\beta_p(124°)$ values of the LISST-VSF were re-calculated by accounting for the angular weigh function of the ECO-BB3 meter.

The histogram distributions of $\beta_p(124°)$ are compared in Fig. 6. $\beta_p(124°)$ measured by the ECO-BB3 varied from 6.7×10^{-5} to 3.8×10^{-4} m^{-1} sr^{-1} with a median of 1.4×10^{-4} m^{-1} sr^{-1}. $\beta_{p,abs}(124°)$ calculated using the absolute calibration varied from 5.6×10^{-5} to 2.1×10^{-4} m^{-1} sr^{-1}, well within the range of the ECO-BB3 measurements, and had a median value of 1.3×10^{-4} m^{-1} sr^{-1}, also very close to the median value estimated from the ECO-BB3 data. In contrast, $\beta_{p,rel}(124°)$ calculated using the relative calibration showed a wide variation, ranging from 3.9×10^{-5} to 5.0×10^{-4} m^{-1} sr^{-1} and a median value of 2.5×10^{-4} m^{-1} sr^{-1}, which deviated significantly from the ECO-BB3 median value.

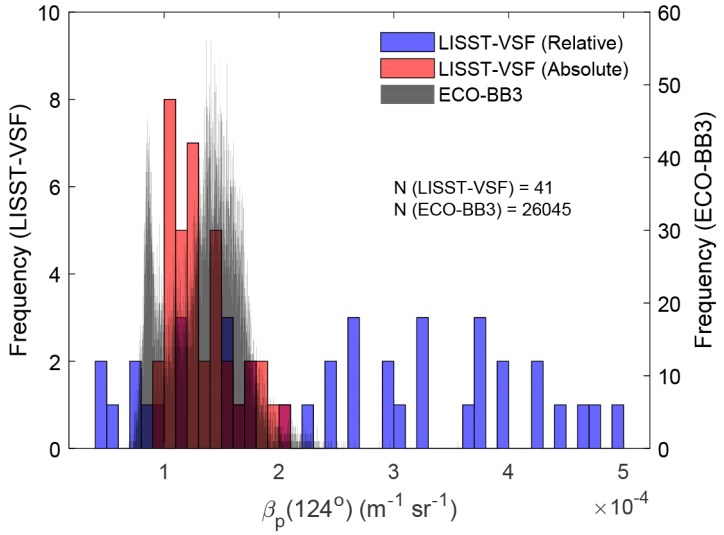

Fig. 6. Histogram distributions of particulate VSF at 124° ($\beta_p(124°)$) calculated from the LISST-VSF (left y-axis) using absolute calibration method developed in this study (red color) and the relative method (blue color) and ECO-BB3 (right y-axis, gray color) in the EX-2018 experiment.

3.3.3. Comparison with ECO-AFL/FL Fluorometer profile

As a further evaluation, we compared b_{bp} obtained using two calibration methods with chlorophyll concentration profiles acquired with a Sea-Bird/WETLab ECO-AFL/FL Fluorometer in two CTD casts during EX-2018 (Fig. 7). Calculation of b_{bp} from LISST-VSF eyeball-measured $\beta_p(\theta)$, which is only available from 15° to 150°, requires the VSF between 150° and 180°. Here, we applied the Zhang et al. [56] two-component model to partition $\beta_p(\theta$=90°-150°) into two end members, one representing the backward scattering by very large particles and the other by very small particles. We then used these two end members to reconstruct the particulate VSF, denoted as $\beta_p^*(\theta)$, whose values between 150° and 180° were used, along with measured $\beta_p(\theta)$ from 90 to

Optics EXPRESS

150°, to calculate b_{bp},

$$b_{bp} = 2\pi \int_{90°}^{150°} \beta_p(\theta) \sin(\theta) d\theta + 2\pi \int_{150°}^{180°} \beta_p^*(\theta) \sin(\theta) d\theta \quad (19)$$

This approach was also used in a recent study by Koestner et al. [28]

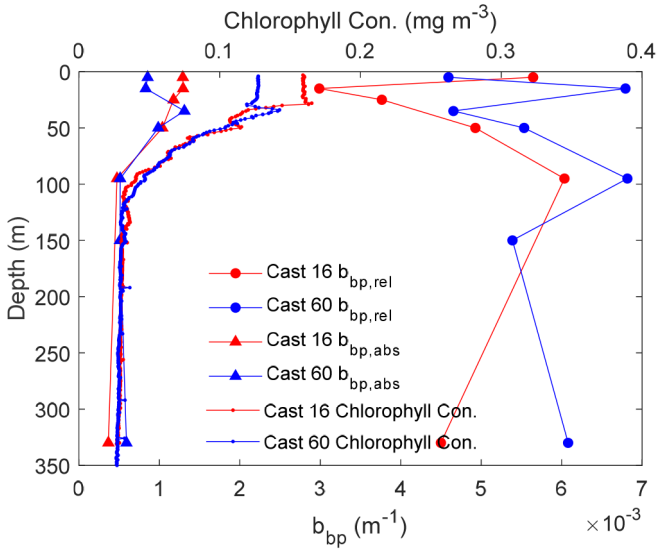

Fig. 7. Comparison of particulate backscattering coefficients (b_{bp}, bottom x-axis) calculated using the absolute calibration method ($b_{bp,abs}$, triangle) and the relative calibration method ($b_{bp,rel}$, circle) at various depths in CDT cast 16 (red lines) and cast 60 (blue lines). The concurrent chlorophyll concentration profile (top x-axis) acquired by a Sea-Bird/WETLab ECO-AFL/FL Fluorometer in two CTD casts overlaid.

The chlorophyll profiles showed a well-mixed water from surface to approximately 30 m at both CTD-16 (red line) and -60 (blue line), and a clear deep chlorophyll maximum at approximately 35-40 m at CTD-60. In both locations, chlorophyll concentration decreased rapidly towards 100 m and then steadily decreased down to 300 m. Clearly, $b_{bp,abs}$ obtained with the absolute calibration method developed in this study, though only at 6–7 discrete depths, mimic the chlorophyll concentration profile very well. On the contrary, the relative method produced $b_{bp,rel}$ profiles that do not match with the observed chlorophyll profiles.

4. Discussion and conclusion

4.1. Uncertainties

The calibration coefficient $\kappa(\theta, 645\,\text{mV})$ was estimated using standard polystyrene beads. The mean diameters of these standard beads are traceable to the NIST, with stated uncertainties (Table 1). These uncertainties in the size of beads would propagate to the determination of $\kappa(\theta, 645\,\text{mV})$. In our experiment using the 0.2 µm beads, the uncertainties in $\kappa(\theta, 645\,\text{mV})$ varied with the scattering angle and had minimums at angles between 110° and 130° with an average coefficient of variation of 0.7% (Fig. 3(b)). The average from these angles is used for $\kappa(645\,\text{mV})$ in this study to minimize the uncertainties associated with the size of the beads. Compared to the size, the uncertainties associated with the imaginary part of the refractive index of the beads (Fig. 1(b)) can be ignored and therefore are not considered further in deriving $\kappa(\theta, 645\,\text{mV})$.

Optics EXPRESS

The other two uncertainties come from the PMT supply voltage and the γ factor when converting P_{11} to the reference voltage in Eq. (12):

$$\left(\frac{\Delta\beta}{\beta}\right)^2 = \gamma^2\left(\frac{\Delta V}{V}\right)^2 + \left(\ln\frac{V}{V_0}\right)^2(\Delta\gamma)^2. \tag{20}$$

The first term in the right-hand side of Eq. (20) represents the uncertainty from the PMT supply voltage, which is unknown, but can be estimated from the repeated measurements. In the calibration experiment (Fig. 3(a)), the gain-converted $P_{11}(60°,645\,\text{mV})$ measured for beads at high concentrations varied only 0.4% over 30 repeated measurements. Assuming that the samples are very well mixed and all the variations in signal are due to fluctuation in the PMT supply voltage, i.e., $\Delta V/V = 0.4\%$, we estimated that $\Delta\beta/\beta \approx 3.4\%$. Accounting for unavoidable heterogeneity of the samples, the actual uncertainty will be less.

The second term of right-hand side of Eq. (20) is the uncertainty due to the γ factor, which is also unknown. However, if PMT supply voltage (V) is the reference voltage (V_0), this uncertainty vanishes. Among a total of 298 measurements collected in the EX-2018 experiment (Table 2), 284 were measured at the PMT supply voltage of 645 mV, and the rest were at 595 and 700 mV. Therefore, we chose 645 mV as the reference voltage to minimize the uncertainty coming from γ in calibration. If the PMT supply voltage is quite different from the reference voltage, for example, at very turbid waters where a much lower supply voltage would be used, caution needs to be taken. Assuming the actual value of γ is 8.0 instead of 8.6 that we used, the uncertainty in calibration will be 5% if the supply voltage is 595 mV while it will be up to 30% if the supply voltage is 400 mV (the smallest voltage). Because we do not know the exact uncertainties associated with the PMT supply voltage and the γ factor, we cannot quantify their impacts on the calibration. However, we believe their impacts are limited, at least over the three PMT voltages of 595,645 and 700 mV that were automatically selected during the calibration (and during the EX-2018 experiment), because the gain-converted P_{11} at 645 mV fit almost linearly against simulated VSF with a correlation coefficient >0.99 (Fig. 3(a)).

In summary, the uncertainty of the absolute calibration is 11.1% based on validation with 0.5 and 11 μm beads that includes the effects of PMT supply voltage and γ factor. Also, we do not recommend to use this absolute calibration if the PMT supply voltage is out of the range of 595, 645, and 700 mV, which may occur in coastal waters.

4.2. β_p (<0.2 μm)

During the EX-2018 experiment, there were 138 samples for which both unfiltered and 0.2 μm-filtered seawater samples were measured by the LISST-VSF. Some of these samples were collected from depths of 300–3000 m. Figure 8(a) shows the bulk VSFs measured by LISST-VSF eyeball component calculated using the new absolute calibration for seawater samples with ($\beta_{<0.2\mu m}$) and without (β) filtration and Fig. 8(b) shows the corresponding particulate VSFs ($\beta_{p,<0.2\mu m}$ and β_p), which were calcualted by subtracting from the bulk VSFs the seawater scattering computed using the Zhang et al. [3] model with concurrently measured temperature and salinity. b_{bp} calcualted from β_p (Eq. 19) varied from 3.1×10^{-4} to 3.0×10^{-3} m^{-1} with a median value of 9.1×10^{-4} m^{-1}, while $b_{bp,<0.2\mu m}$ calculated from $\beta_{p,<0.2\mu m}$ varied from 1.2×10^{-4} to 3.3×10^{-4} m^{-1} with a median value of 2.0×10^{-4} m^{-1}. The relative contribution of very small particles (<0.2 μm) (measured as the ratio of $b_{bp,<0.2\mu m}$ to b_{bp}) ranged from 6.4% to 56.8% with an average of 26.7%. Fully investigating scattering by very small particles will be reported in a separate paper and is beyond the scope of this study. Here, we would like to point out several features shown in Fig. 8 that pertain to this study. First, $\beta_{<0.2\mu m}$ includes contribution by seawater and as expected its values calculated from the measurements are almost always greater than those by seawater as can be seen by comparison of red curves and the black curve in Fig. 8(a). This indicates the calibration scheme developed in this study is physically sound. Second, $\beta_{p,<0.2\mu m}$ in clear oceanic waters is

Optics EXPRESS

generally less than the scattering due to pure seawater but not negligible. Therefore, one should avoid using the blank-subtraction method or be aware of its implication in studying particle scattering in these type of waters. However, we do acknowledge that the blank-subtraction method, which is commonly used in routine measurements of inherernt optical properties of seawater, such as by an ac-meter measuring bulk absorption/attenuaiton coefficients[57] or a UV-VIS spectrophotometer measuring absorption of dissolved material [58], does offer an advantage of correcting for the drift of the instrument or potential instrumental bias. Third, for instruments to be able to resolve the backscattering by very small particles, the sensitivity should be on the order of 1/10 of the scattering due to seawater (e.g, comparing red curves and the black curve in Fig. 8(b)).

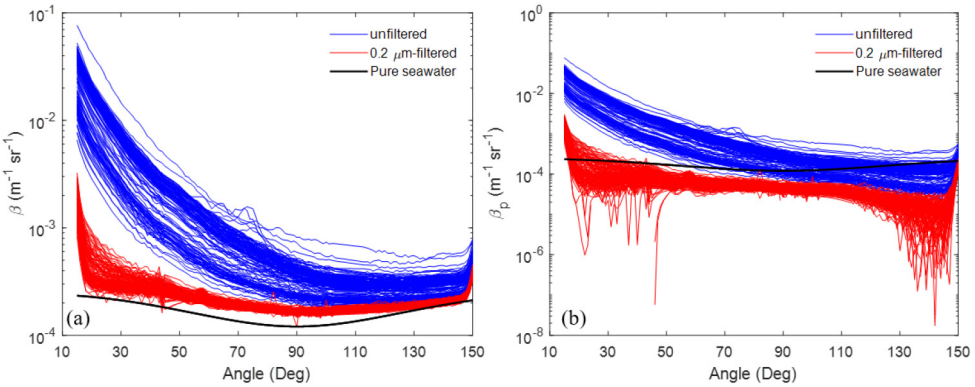

Fig. 8. (a) Measured bulk VSFs (β) by LISST-VSF eyeball component calculated using the absolute calibration for unfiltered (blue lines) and 0.2 µm-filtered (red lines) seawater samples collected in the EX-2018 experiment. The VSF of pure seawater (β_{sw}, black line) calculated from the theoretical model (λ=517 nm, $T = 15°$, $S = 33$ PSU) [3] is overlaid. (b) Same as (a) but for particulate VSFs (β_p).

4.3. Selection of calibration methods

For applications in clear oceanic waters, we recommend the use of absolute calibration method developed in this study because the relative calibration method may fail due to low signal-to-noise ratio for the LISST ring detectors in these type of waters (Figs. 5–7). For historic LISST-VSF data measured in these types of waters, we suggest to conduct a calibration experiment similar to ours to determine the absolute calibration coefficient for the specific eyeball component and re-process these data. Furthermore, we recommend refraining from using blank subtraction because the contribution of very small particles (< 0.2 µm) to total backscattering cannot be neglected in such waters (section 4.2). In other oceanic or coastal waters (e.g., $0.1 < \beta_p(15°) < 1\ m^{-1}\ sr^{-1}$), the VSFs calculated using the two calibration methods agree with each other well and therefore either one can be used (Fig. 5). For more turbid waters, we recommend the relative calibration method for two reasons. First, in turbid waters, it is likely that a PMT supply voltage lower than the range encountered in this study will be applied, and uncertainty from the γ factor could be significant (see section 4.1). Second, the forward scattering in coastal waters is normally sufficient for ring detectors to generate valid signals that can be used for calibration.

The absolute calibration method developed in this study extends the use of the LISST-VSF instrument to clear waters, where the default, relative calibration method tends to fail. Even though the calibration coefficient derived in this study can only be used for the specific LISST-VSF instrument that we have, the methodology can be easily applied to other LISST-VSF instruments.

Optics EXPRESS

Funding

National Aeronautics and Space Administration (NASA) (80NSSC17K0656, 80NSSC18M0024, NNX15AC85G); National Science Foundation (NSF) (1917337); National Natural Science Foundation of China (NSFC) (61675187).

Acknowledgements

We thank Wayne Slade, Thomas Leeuw, and David Dana with Sequoia Scientific for helping us to better understand the LISST-VSF instrument and data processing code. We also thank two anonymous reviewers for their comments and suggestions that have helped us to improve the manuscript.

References

1. C. Mobley, *Light and Water: Radiative Transfer in Natural Waters* (Academic Press., 1994).
2. X. Zhang and L. Hu, "Estimating scattering of pure water from densityfluctuation of the refractive index," Opt. Express **17**(3), 1671–1678 (2009).
3. X. Zhang, L. Hu, and M.-X. He, "Scattering by pure seawater: Effect of salinity," Opt. Express **17**(7), 5698–5710 (2009).
4. L. Hu, X. Zhang, and M. J. Perry, "Light scattering by pure seawater: Effect of pressure," Deep Sea Res., Part I **146**, 103–109 (2019).
5. J. R. V. Zaneveld, J. C. Kitchen, A. Bricaud, and C. C. Moore, "Analysis of in-situ spectral absorption meter data," in *San Diego '92*, (SPIE, 1992), 14.
6. T. J. Petzold, "Volume scattering functions for selected ocean waters," Report (Scripps Institution of Oceanography), 72–78 (1972).
7. G. Kullenberg, "Scattering of light by Sargasso Sea water," Deep-Sea Res. Oceanogr. Abstr. **15**(4), 423–432 (1968).
8. J. E. Tyler and W. H. Richardson, "Nephelometer for the Measurement of Volume Scattering Function in Situ," J. Opt. Soc. Am. **48**(5), 354–357 (1958).
9. C. D. Mobley, L. K. Sundman, and E. Boss, "Phase function effects on oceanic light fields," Appl. Opt. **41**(6), 1035–1050 (2002).
10. S. Sathyendranath and T. Platt, "Analytic model of ocean color," Appl. Opt. **36**(12), 2620–2629 (1997).
11. Z. Lee, K. L. Carder, C. D. Mobley, R. G. Steward, and J. S. Patch, "Hyperspectral Remote Sensing for Shallow Waters. I. A Semianalytical Model," Appl. Opt. **37**(27), 6329–6338 (1998).
12. K. J. Voss and E. S. Fry, "Measurement of the Mueller matrix for ocean water," Appl. Opt. **23**(23), 4427–4439 (1984).
13. H. Volten, J. F. de Haan, J. W. Hovenier, R. Schreurs, W. Vassen, A. G. Dekker, H. J. Hoogenboom, F. Charlton, and R. Wouts, "Laboratory measurements of angular distributions of light scattered by phytoplankton and silt," Limnol. Oceanogr. **43**(6), 1180–1197 (1998).
14. E. S. Fry and K. J. Voss, "Measurement of the Mueller matrix for phytoplankton1," Limnol. Oceanogr. **30**(6), 1322–1326 (1985).
15. M. S. Quinby-Hunt, A. J. Hunt, K. Lofftus, and D. Shapiro, "Polarized-light scattering studies of marine Chlorella," Limnol. Oceanogr. **34**(8), 1587–1600 (1989).
16. K. J. Voss, W. M. Balch, and K. A. Kilpatrick, "Scattering and attenuation properties of Emiliania huxleyi cells and their detached coccoliths," Limnol. Oceanogr. **43**(5), 870–876 (1998).
17. K. Witkowski, T. Król, A. Zieliriński, and E. Kuteń, "A light-scattering matrix for unicellular marine phytoplankton," Limnol. Oceanogr. **43**(5), 859–869 (1998).
18. M. E. Lee and M. R. Lewis, "A New Method for the Measurement of the Optical Volume Scattering Function in the Upper Ocean," J. Atmos. Ocean. Technol. **20**(4), 563–571 (2003).
19. J. K. Lotsberg, E. Marken, J. J. Stamnes, S. R. Erga, K. Aursland, and C. Olseng, "Laboratory measurements of light scattering from marine particles," Limnol. Oceanogr.: Methods **5**(1), 34–40 (2007).
20. J.-F. Berthon, E. Shybanov, M. E. G. Lee, and G. Zibordi, "Measurements and modeling of the volume scattering function in the coastal northern Adriatic Sea," Appl. Opt. **46**(22), 5189–5203 (2007).
21. J. M. Sullivan and M. S. Twardowski, "Angular shape of the oceanic particulate volume scattering function in the backward direction," Appl. Opt. **48**(35), 6811–6819 (2009).
22. M. Twardowski, X. Zhang, S. Vagle, J. Sullivan, S. Freeman, H. Czerski, Y. You, L. Bi, and G. Kattawar, "The optical volume scattering function in a surf zone inverted to derive sediment and bubble particle subpopulations," J. Geophys. Res.: Oceans **117**(C7), 7347 (2012).
23. M. Babin, D. Stramski, R. A. Reynolds, V. M. Wright, and E. Leymarie, "Determination of the volume scattering function of aqueous particle suspensions with a laboratory multi-angle light scattering instrument," Appl. Opt. **51**(17), 3853–3873 (2012).

Optics EXPRESS

24. C. Li, W. Cao, J. Yu, T. Ke, G. Lu, Y. Yang, and C. Guo, "An Instrument for In Situ Measuring the Volume Scattering Function of Water: Design, Calibration and Primary Experiments," Sensors (Basel, Switzerland) **12**(4), 4514–4533 (2012).
25. H. Tan, R. Doerffer, T. Oishi, and A. Tanaka, "A new approach to measure the volume scattering function," Opt. Express **21**(16), 18697–18711 (2013).
26. M. Chami, A. Thirouard, and T. Harmel, "POLVSM (Polarized Volume Scattering Meter) instrument: an innovative device to measure the directional and polarized scattering properties of hydrosols," Opt. Express **22**(21), 26403–26428 (2014).
27. W. H. Slade, Y. C. Agrawal, and O. A. Mikkelsen, "Comparison of measured and theoretical scattering and polarization properties of narrow size range irregular sediment particles," in *OCEANS - San Diego*, (IEEE, 2013), 1-6.
28. D. Koestner, D. Stramski, and R. A. Reynolds, "Measurements of the Volume Scattering Function and the Degree of Linear Polarization of Light Scattered by Contrasting Natural Assemblages of Marine Particles," Appl. Sci. **8**(12), 2690 (2018).
29. Y. C. Agrawal and O. A. Mikkelsen, "Empirical forward scattering phase functions from 0.08 to 16 deg. for randomly shaped terrigenous 1–21 μm sediment grains," Opt. Express **17**(11), 8805–8814 (2009).
30. Y. C. Agrawal, "The optical volume scattering function: Temporal and vertical variability in the water column off the New Jersey coast," Limnol. Oceanogr. **50**(6), 1787–1794 (2005).
31. T. W. Chen, "Simple formula for light scattering by a large spherical dielectric," Appl. Opt. **32**(36), 7568–7571 (1993).
32. G. R. Fournier and L. J. Forand, "Analytic phase function for ocean water," in *Ocean Optics XII*, (SPIE, 1994), 8.
33. D. Stramski and D. A. Kiefer, "Light scattering by microorganisms in the open ocean," Prog. Oceanogr. **28**(4), 343–383 (1991).
34. D. Stramski and S. B. Woźniak, "On the role of colloidal particles in light scattering in the ocean," Limnol. Oceanogr. **50**(5), 1581–1591 (2005).
35. X. Zhang and D. J. Gray, "Backscattering by very small particles in coastal waters," J. Geophys. Res.: Oceans **120**(10), 6914–6926 (2015).
36. D. Stramski, E. Boss, D. Bogucki, and K. J. Voss, "The role of seawater constituents in light backscattering in the ocean," Prog. Oceanogr. **61**(1), 27–56 (2004).
37. Sequoia Scientific Inc., "LISST-VSF user's manual (Version 3.0)," https://www.sequoiasci.com/product/lisst-vsf/ (2016).
38. X. Zhang, D. Stramski, R. A. Reynolds, and E. R. Blocker, "Light scattering by pure water and seawater: the depolarization ratio and its variation with salinity," Appl. Opt. **58**(4), 991–1004 (2019).
39. E. Boss, W. S. Pegau, M. Lee, M. Twardowski, E. Shybanov, G. Korotaev, and F. Baratange, "Particulate backscattering ratio at LEO 15 and its use to study particle composition and distribution," *J. Geophys. Res. Oceans* 109 (2004).
40. G. Dall'Olmo, T. K. Westberry, M. J. Behrenfeld, E. Boss, and W. H. Slade, "Significant contribution of large particles to optical backscattering in the open ocean," Biogeosciences **6**(6), 947–967 (2009).
41. J. M. Sullivan, M. S. Twardowski, J. Ronald, V. Zaneveld, and C. C. Moore, "Measuring optical backscattering in water," in Light Scattering Reviews 7: Radiative Transfer and Optical Properties of Atmosphere and Underlying Surface, A. A. Kokhanovsky, ed. (Springer Berlin Heidelberg, Berlin, Heidelberg, 2013), pp. 189-224.
42. W. H. Slade and E. S. Boss, "Calibrated near-forward volume scattering function obtained from the LISST particle sizer," Opt. Express **14**(8), 3602–3615 (2006).
43. T. Harmel, M. Hieronymi, W. Slade, R. Röttgers, F. Roullier, and M. Chami, "Laboratory experiments for inter-comparison of three volume scattering meters to measure angular scattering properties of hydrosols," Opt. Express **24**(2), A234–A256 (2016).
44. C. F. Bohren and D. R. Huffman, *Absorption and Scattering of Light by Small Particles* (John Wiley, New York, 1983).
45. X. Ma, Q. J. Lu, R. S. Brock, M. K. Jacobs, P. Yang, and X.-H. Hu, "Determination of complex refractive index of polystyrene microspheres from 370 to 1610 nm," Phys. Med. Biol. **48**(24), 4165–4172 (2003).
46. A. Quirantes, F. Arroyo, and J. Quirantes-Ros, "Multiple Light Scattering by Spherical Particle Systems and Its Dependence on Concentration: A T-Matrix Study," J. Colloid Interface Sci. **240**(1), 78–82 (2001).
47. S.-K. Chae and H. S. Lee, "Determination of Radiative Transport Properties of Particle Suspensions by a Single-Scattering Experiment," Aerosol Sci. Technol. **18**(4), 389–402 (1993).
48. M. S. Twardowski, H. Claustre, S. A. Freeman, D. Stramski, and Y. Huot, "Optical backscattering properties of the "clearest" natural waters," Biogeosciences **4**(6), 1041–1058 (2007).
49. H. Freeland, "A short history of Ocean Station Papa and Line P," Prog. Oceanogr. **75**(2), 120–125 (2007).
50. C. S. Wong, Z. Yu, N. A. D. Waser, F. A. Whitney, and W. K. Johnson, "Seasonal changes in the distribution of dissolved organic nitrogen in coastal and open-ocean waters in the North East Pacific: sources and sinks," Deep Sea Res., Part II **49**(24-25), 5759–5773 (2002).
51. D. A. Siegel, K. O. Buesseler, M. J. Behrenfeld, C. R. Benitez-Nelson, E. Boss, M. A. Brzezinski, A. Burd, C. A. Carlson, E. A. D'Asaro, S. C. Doney, M. J. Perry, R. H. R. Stanley, and D. K. Steinberg, "Prediction of the Export and Fate of Global Ocean Net Primary Production: The EXPORTS Science Plan," *Front. Mar. Sci.* 3 (2016).

Optics EXPRESS

52. P. W. Holland and R. E. Welsch, "Robust regression using iteratively reweighted least-squares," Commun. Stat. Theor. M. **6**(9), 813–827 (1977).
53. P. Werdell and S. Bailey, "The SeaWiFS Bio-optical Archive and Storage System (SeaBASS): Current Architecture and Implementation," Technical Report, NASA, Goddard Space Flight Center (2002).
54. E. Boss, "SeaWiFS Bio-optical Archive and Storage System (SeaBASS)," NASA, Accessed: 10 February, 2019.
55. E. Boss, L. Guidi, M. J. Richardson, L. Stemmann, W. Gardner, J. K. B. Bishop, R. F. Anderson, and R. M. Sherrell, "Optical techniques for remote and in-situ characterization of particles pertinent to GEOTRACES," Prog. Oceanogr. **133**, 43–54 (2015).
56. X. Zhang, G. R. Fournier, and D. J. Gray, "Interpretation of scattering by oceanic particles around 120 degrees and its implication in ocean color studies," Opt. Express **25**(4), A191–A199 (2017).
57. IOCCG Protocol Series, "Inherent optical property measurements and protocols: absorption coefficient, Neeley, A.R., and Mannino, A.(eds.)," IOCCG ocean optics and biogeochemistry protocols for satellite ocean colour sensor validation (2018).
58. J. L. Mueller, G. S. Fargion, M. C. R. , S. Pegau, Z. J. R. V. , B. G. Mitchell, K. Mati, J. Wieland, and M. Stramska, "Ocean optics protocols for satellite ocean color sensor validation, revision 4, volume IV: inherent optical properties: instruments, characterizations, field measurements and data analysis protocols," NASA Tech. Memo NASA/TM-2003-211621/Rev4-Vol.IV (2003).